Magnetization of Superconducting Nb–25%Zr Wire

W. A. FIETZ, M. R. BEASLEY, J. SILCOX, AND W. W. WEBB
Department of Engineering Physics and Materials Science
and
Laboratory of Atomic and Solid State Physics, Cornell University, Ithaca, New York
(Received 18 May 1964)

The magnetization and critical transport-current densities of samples of superconducting niobium–25% zirconium cold-worked wire have been measured quantitatively up to 40 kOe applied field. All of the magnetization characteristics, as measured by several techniques, and the critical transport currents conform to critical-state concepts provided that the equilibrium magnetization is included in the analysis. The equilibrium magnetization curves could be deduced from the hysteretic measured magnetization data, and the results agree with the theory of Abrikosov for type-II superconductors. The irreversible magnetization-current densities $J_c(B)$, where B is the local magnetic induction, just equal the critical transport-current densities $J_t(H)$ in the range 4 to 40 kOe applied field. They are accurately fitted by an empirical critical-state expression of the form $J_c(B)=a_o \exp(-B/b_o)+c_o$ where a_o, b_o, and c_o are measured constants of the material. The methods used appear to be generally applicable to the study of hysteretic superconducting wire.

1. INTRODUCTION

THE concept of the critical state has made high-current, high-field superconductors qualitatively understandable. Bean,[1] Kim, Hempstead, and Strnad[2,3] and Anderson[4] have introduced the idea of the critical state and it is now clear[5] that it has unique features, particularly high critical supercurrent densities, that are separate and additional to the flux penetration, absence of the Meissner effect, and high upper critical field that characterize the equilibrium, type-II superconductors of Abrikosov.[6]

Concurrently with the evolution of the concept of the critical state, an intricate technology has yielded high-current, high-field superconducting wire. However, quantitative application of critical-state concepts to these materials has been hampered by the fact that the characteristics depend strongly on the processing involved in reducing them to wire form so that relevant measurements must be made on wire. A popular material has been a heavily cold-worked alloy of niobium with 25% zirconium (Nb–25%Zr) and various interstitial condiments,[7] that displays a collection of bizarre phenomena.[8] For this alloy there are innumerable data on critical transport currents but only qualitative measurements of the magnetization of the wire at low applied fields have been reported.[9,10]

The objective of this paper is a detailed test of the applicability of critical-state concepts to Nb–25%Zr superconducting wire. With this objective, measurements of magnetization and differential susceptibility by three methods, and of critical transport currents were carried out up to 40 kOe, and the necessary analysis for specimens in the form of solenoidal coils was worked out. In Sec. 2 the experimental methods and the relations between the observable quantities and the average magnetization in the critical state are discussed for this rather unconventional geometry. In Sec. 3, an analysis of critical-state relations is presented. In Subsection 3.2 the field-dependent equilibrium magnetization is introduced into the critical-state formulation; in 3.3 the relevant relations of the critical current density $J_c(B)$ as given by a "critical-state equation" to the average magnetization M are worked out for the geometry of a simply connected solenoidal coil of wire, and in 3.4 and 3.5 the procedures for deducing the critical-state equation from the experimental results are worked out. Results on Nb–25%Zr wire follow in Sec. 4 where the critical-state equation and its material parameters, the equilibrium magnetization, the critical-transport currents and some additional characteristics of the critical state in this material are reported. General conclusions follow in Sec. 5.

2. EXPERIMENTS

2.1. Program

The average magnetizations of several small coils of superconducting wire were determined in these experiments as functions of applied magnetic field and magnetic history at 4.2°K. Measurements of changes of flux through appropriate pickup coils during changes of

[1] C. P. Bean, Phys. Rev. Letters **8**, 250 (1962).
[2] Y. B. Kim, C. F. Hempstead, and A. R. Strnad, Phys. Rev. Letters **9**, 306 (1962).
[3] Y. B. Kim, C. F. Hempstead, and A. R. Strnad, Phys. Rev. **129**, 528 (1963).
[4] P. W. Anderson, Phys. Rev. Letters **9**, 309 (1962).
[5] T. G. Berlincourt and R. R. Hake, Phys. Rev. **131**, 140 (1963).
[6] A. A. Abrikosov, Zh. Eksperim. i Teor. Fiz. **32**, 1442 (1957) [English transl.: Soviet Phys.—JETP **5**, 1174 (1957)].
[7] See, for example, J. E. Kunzer, Bull. Am. Phys. Soc. **6**, 298 (1961); T. G. Berlincourt, R. R. Hake, and D. H. Leslie, Phys. Rev. Letters **6**, 671 (1961); J. E. Kunzler, Rev. Mod. Phys. **33**, 501 (1961).
[8] See, for example, H. Riemersma, J. K. Hulm, A. J. Venturino, and B. S. Chandrasekhar, J. Appl. Phys. **33**, 3499 (1962); J. K. Hulm, B. S. Chandrasekhar, and H. Riemersma, *1962 Cryogenics Conference* (University of California Press, Berkley, California, 1962).
[9] M. A. R. LeBlanc, Phys. Letters **6**, 140 (1963).
[10] D. C. Montgomery, IEEE Spectrum, 103 (February 1964).

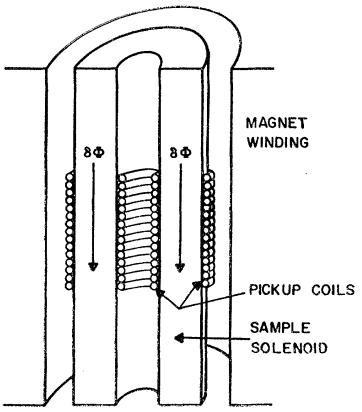

FIG. 1. The arrangement of the pickup coils for the magnetization measurement.

applied magnetic field yielded values of average differential susceptibility $\bar{\chi}_\Delta(H)$ which were integrated to yield the complete set of values of average specimen magnetization $4\pi\bar{M}(H)$ as functions of applied field and magnetic history. Responses to applied field changes, both as steps of various sizes and as continuous functions of time, defined the range of uniqueness of the apparent susceptibility and magnetization values.

Independent determinations of magnetization were obtained by thermal demagnetization; that is, by measuring the changes in flux through pickup coils as all superconductivity was destroyed by warming specimens above their critical temperature in steady magnetic fields. The field dependence of the critical transport currents of the same specimens as a function of applied magnetic field was determined by adjusting the applied field to establish the specimen at the desired point of the critical-state curve, then raising the transport current until a normal transition occurred.

2.2. Procedures

2.2.1. Specimen Preparation

The specimens, in the form of long, open-circuited, multilayer solenoids, were wound from samples of commercial niobium-25% zirconium alloy. Each specimen consisted of about 10 layers of wire forming a solenoid with the nominal dimensions; inside diameter 1 cm, outside diameter 2 cm, length 12 cm. From each material two of these coils were wound, one inductively, and the other in noninductive, bifilar form for critical current measurements. Mylar sheets were inserted between layers of the windings but for the material without organic insulation, adjacent turns in the same layer were in electrical contact through the copper plating on the wire. The ends of the specimen coils, although open-circuited during magnetization measurements, were led outside the high-field region to tinned copper compression blocks for connection to current leads for transport current measurements.

Pickup coils were placed inside and outside the specimen as shown in Fig. 1, and a noninductive heater coil with removable thermal insulation surrounded the whole arrangement.

2.2.2. Measurements

The outer and inner concentric coils shown in Fig. 1 each consisted of N turns (N being 10 or 400) enclosing areas A_1 and A_2. The coils were connected in opposition, so that the deflection of a fluxmeter connected across the coils was directly proportional to N and to the change of flux through the area A_1-A_2 between the coils. A General Electric fluxmeter with a galvanometer constant of 96 G cm^2 per mm deflection indicated flux changes during incremental applied field changes and thermal demagnetizations. For continuous applied field changes, an integrating circuit using two Dymec Model DY-2460-A dc amplifiers was arranged to plot directly on an X-Y recorder the quantity $4\pi\bar{M}$ as a function of applied field.

The magnetic field was provided by superconducting solenoids with field capabilities of 40 kOe. To provide the precise current control required for step increments of applied field a transistorized regulator was used with storage batteries. It provided current steps adjustable so that any field increment from 10 to 1000 Oe could be obtained. The stability of the regulator was sufficient to maintain any field setting to within ± 1.5 Oe over the operating range of the magnet for periods of time of the order of hours. Variation of the time rate of change of applied field steps by a factor of five produced no observable differences in the recorded data. In general, the larger steps (750 Oe) were about 95% complete in 0.5 sec with no overshoot.

2.3. Analysis of Measurements

In this section the relations needed to compute the average magnetization $4\pi\bar{M}$ from the experimental data are derived. Parameters characteristic of the material are deduced from average magnetization values by relations given in Sec. 3.

2.3.1. Differential Susceptibility

These measurements are conveniently expressed in terms of an experimental parameter δ, the ratio of fluxmeter deflection d, to the change in magnet current ΔI_s. This ratio in turn is proportional to the ratio of the change of flux through the sensing coils $\Delta\varphi$, to the change in the applied field ΔH_a. Thus,

$$\delta = d/\Delta I_s = K\Delta\varphi/\Delta H_a. \tag{2.1}$$

The measurable constant of proportionality $K = k_1 k_2$, incorporates the fluxmeter sensitivity and coil geometry in $k_1 = d/\Delta\varphi$, and the magnet constant in $k_2 = \Delta H_a/\Delta I_s$.

The open-circuited solenoid specimens are simply connected. Therefore, a simple relation holds approximately between the flux through the area A of the pickup coils and the average magnetization $\bar{M}$, per unit volume of the material in an applied field H_a.

This is

$$\varphi/A = H_a + 4\pi f \bar{M}, \tag{2.2}$$

where f is a factor that accounts for the demagnetization and other geometrical corrections. In the case of a single solid ellipsoidal specimen of soft superconductor in a uniform applied field, f is a constant independent of H_a as in the careful analysis of Cochran, Mapother, and Mould.[11]

For this special case Eqs. (2.1) and (2.2) yield

$$\delta = KA(1 + 4\pi f d\bar{M}/dH_a). \tag{2.3}$$

The limiting case with the material normal defines

$$\delta_n = KA, \tag{2.4}$$

and with the material perfectly diamagnetic

$$\delta_d = KA(1-f). \tag{2.5}$$

Combining Eqs. (2.3)–(2.5) yields a convenient expression for the average differential susceptibility $\bar{\chi}_\Delta = d\bar{M}/dH$ if the demagnetization effects represented by $dH/dH_a = (1-n)^{-1} \approx 1$ can be neglected. Thus, in the relation

$$4\pi\bar{\chi}_\Delta = (\delta - \delta_n)/(\delta_n - \delta_d), \tag{2.6}$$

the quantities, f, K, and A cancel out if the demagnetization factor $n \ll 1$.

Clearly the application of Eq. (2.6) to more complex cases would be convenient and useful if it is a justifiable approximation. It would be sufficient to show that an effective demagnetization factor is definable and that the effects of changes of f and n with $\bar{M}$ are negligible.

In strictly diamagnetic behavior with $\mathbf{M}$ parallel to $\mathbf{H}_a$, an effective demagnetization factor n_d is definable by

$$n_d = \frac{1}{4\pi\bar{M}}\left(\mathbf{H}_a - \frac{1}{V}\int_v \mathbf{H}(\mathbf{r})d^3r\right), \tag{2.7}$$

where $\mathbf{H}(\mathbf{r})$ is the local magnetic field and the integral is over the volume of the superconducting material. A graphical solution for the field distribution in and around a row of diamagnetic wires corresponding to one layer of a solenoid gave $n_d \leqq 0.06$ and a maximum field at the wire surface of $H_{\max} \cong 1.2H_a$.

Experimental determinations of the effective demagnetization factor n_d were obtained by comparing measurements of the absolute magnetic moment in the diamagnetic regions with values calculated assuming ideal diamagnetic behavior. Within the $\pm 3\%$ experimental error of measurement (limited by dimensional measurements) the demagnetization factor $n_d \cong 0$.

This helpful result can be understood by recognizing the specimen solenoids as geometrically equivalent to sheets of superconducting material with surfaces parallel to the applied field but roughened by transverse corrugations corresponding to individual wires. A sheet of comparable dimensions has a demagnetization factor between 0.002 and 0.04. End effects are remote from the pickup coils and the main effect of the roundness of the wire is a surface roughness. The field perturbations due to adjacent layers decay rapidly with distance from the wire surfaces and were estimated to be less than 10% of H_a.

Now in regions where flux penetrates the specimen, nonuniform magnetization is expected from the nature of the critical state. In general, a consequence of nonuniform magnetization is a demagnetizing field that is not parallel to the local magnetization. Thus, the demagnetizing factor should be generalized to have a tensor character. Alternatively, the scalar n_d can be retained to represent the component of demagnetizing field parallel to $\mathbf{H}_a$ and a vector demagnetizing coefficient $\mathbf{n}_p$ can be introduced to represent the component of the demagnetizing field perpendicular to $\mathbf{M}$ in the form $4\pi(\mathbf{n}_p \times \mathbf{M})$. An average effective value of $|\mathbf{n}_p|$ can be defined in analogy with Eq. (2.7). Symmetry considerations suggest that it would be small. A complete solution of this problem to verify this conclusion would be prohibitively lengthy. Instead, the lead of other workers[2,3] is followed in assuming that, since our demagnetizing effects are negligibly small for the diamagnetic case, they are also negligible in the nonuniform magnetization region. This assumption is most likely to break down in the region of the steepest flux gradients, i.e., in low-field penetration, and will progressively improve as the flux gradients become less steep in higher fields.

2.3.2. *Magnetization by Integration of* $\bar{\chi}_\Delta$

Complete magnetization curves can be derived from a set of measurements of differential susceptibility obtained by systematically varying the applied field starting at $H_a = M = 0$. Then the magnetization at any point is given by integration of the differential susceptibility along the curve $\bar{\chi}_\Delta(H_a)$. However, this method suffers from the fact that the errors in $\bar{\chi}_\Delta(H_a)$ are cumulative in $\bar{M}(H_a)$ so that serious discrepancies can occur after a period of summation or integration. To eliminate this problem, values of $\bar{M}(H_a)$ at equal values of H_a in two parts of the hysteresis loop were forced to agree precisely with the directly measured values of $\bar{M}(H_a)$ at this field by slight adjustment of the parameter δ_n. To accomplish this, a best value δ_n was calculated using thermal demagnetization data (see next section) at fields around 12 kOe. For each specimen three values of δ_n calculated from thermal demagnetization at six different field points agreed with each other to within 0.1%. These values fell within the 1.5% uncertainty of direct measurements of δ_n at 77°K and within the 3% precision of values calculated from coil geometry.

[11] J. F. Cochran, D. E. Mapother, and R. E. Mould, Phys. Rev. 103, 1657 (1956).

2.3.3. Direct Magnetization Measurements

Heating the superconducting specimens above their critical temperature to destroy magnetization provided a direct measure of the average magnetization of the specimen immediately prior to heating. The fluxmeter deflection d_m, observed during transition in constant applied field provides a measure of this magnetization. Noting that $d_m=k_1\Delta\varphi$, use of Eq. (2.2), (2.4), and (2.5) expresses the magnetization in terms of the measured quantities as

$$4\pi\bar{M}=d_m k_2/(\delta_n-\delta_d). \tag{2.8}$$

This method, which is identical to that of LeBlanc[9] was used for the standardization of $\bar{X}(H)$ measurements mentioned above, and for selected field points.

2.3.4. Errors

Drift of the fluxmeter pickup coil combination was consistently less than 1 mm/sec and could be reduced by another order of magnitude over a part of the scale when required. Although this drift might hide some slow changes of specimen magnetization, such effects were not found in independent checks. Thus, the actual measurement of incremental flux changes are probably accurate to about 2% or twice the reading error of the fluxmeter. With the standardization procedure previously mentioned, it is believed that the errors of measurement are $<5\%$. However, the assumptions of constant effective demagnetization factor equal to 0 and the limits of reproducibility of sample behavior introduce substantially larger uncertainties. All told, uncertainties of about 10% in $\bar{\chi}_\Delta(H_a)$ and $\bar{M}(H_a)$ are expected.

3. THE CRITICAL STATE

3.1. Basis for the Critical State

The existence of a critical state follows from the assumption that the material is capable of sustaining virtually lossless currents up to a critical current density J_c, but not beyond. If this magnitude of current flows everywhere in the specimen, it is said to be in the critical state. It is assumed that there exists a relationship $J_c(B)$ such that the critical current is determined solely by the value of the magnetic induction B at that point.

This idea was employed by Bean[1] to qualitatively explain some of the features of a hysteretic superconductor assuming $J_c=$const. Kim, Hempstead, and Strnad[2] used the critical-state equation $J_c=\alpha/(B+B_0)$ to discuss the magnetization of hollow superconducting cylinders. Although the critical state has been related to the pinning of fluxoids by specific structural features by Rollins and Silcox,[12] by Friedel, Matricon, and DeGennes,[13] and by Webb,[14] no universal critical-state equation has been established. In order to provide a specific function for comparison with experiment, the two forms above are combined and generalized to the form

$$J_c=\frac{a_0}{b_0+B+b_2B^2+b_3B^3+\cdots}$$
$$+c_0+c_1B+c_2B^2+\cdots. \tag{3.1}$$

Since the critical-state current must also obey Maxwell's equation, $\nabla\times\mathbf{B}=k\mathbf{J}$, the possible internal fields and the current distributions are in principle determined if the material is in the critical state. The value of k is $4\pi/10$ for B in gauss and J in amperes cm^{-2}. For the particular case of a large flat plate with an applied field parallel to its surface, this becomes

$$\pm\int_{H_a}^{B(x)}\frac{dB}{J(B)}=kx, \tag{3.2}$$

where x is measured from the nearest surface of the material, and the $\pm$ sign arises in writing the vector relationship as a scalar equation.

If the form of the critical-state equation is known, it may be inserted in Eq. (3.2) to obtain the functional form of $B(x)$. Then, using the symmetry about the center of the flat plate, the possible values of average magnetization of such a sample can be calculated by integrating the quantity $[B(x)-H_a]/w$ over one-half the specimen, where $2w$ is the specimen thickness.

3.2. The Equilibrium Magnetization

The equilibrium magnetization is not explicitly incorporated in the critical-state equation used above. In Bean's original model with J_c constant, only the complete diamagnetism of the matrix at low fields was included. These critical-state equations predict symmetry about the $\bar{M}=0$ axis at high fields whereas many data are asymmetric at high fields. An asymmetric contribution is expected for any type-II superconductor from the models of Abrikosov[6] or of Goodman[15] and the Ginsburg-Landau[16] theory. In order to incorporate the equilibrium magnetization in the critical-state formulation, it is associated with an equivalent surface current J_e that is assumed to be independent of the critical-state magnetization so that it depends only on the magnitude of the applied field in the region adjacent to the superconductor surface.

The equilibrium magnetization M_e is included by breaking the integral of Eq. (3.2) into two parts, one over the equilibrium surface current J_e, and one over the bulk material. Considering that the surface currents extend at most over a distance of the order of a London penetration depth, the first integral is negligible, and

[12] J. Silcox and R. W. Rollins, Appl. Phys. Letters **2**, 231 (1963).
[13] J. Friedel, P. G. DeGennes, and J. Matricon, Appl. Phys. Letters **2**, 119 (1963).
[14] W. W. Webb, Phys. Rev. Letters **11**, 191 (1963).
[15] B. B. Goodman, IBM J. Res. Develop. **6**, 63 (1962).
[16] J. L. Ginsberg and L. D. Landau, Zh. Eksperim. i Teor. Fiz. **20**, 1064 (1950).

Eq. (3.2) becomes

$$\pm\int_{H_a+4\pi M_e}^{B(x)} \frac{dB}{J(B)} = kx. \qquad (3.3)$$

It will be noticed that the only effect of the equilibrium magnetization is to change the lower limit of the integration from H_a to $H_a+4\pi M_e$, which is denoted H_0 hereafter.

3.3. The Critical State in Simply Connected Material

To apply critical-state theory to the magnetization of the geometrically complex coils of wire discussed in this paper seems at first formidable. However, the simple geometry of a flat plate is a remarkably good approximation for the open-circuited layer wound solenoid. The open-circuited coil is a simply connected specimen (in contrast with the hollow cylinders often used to study the critical state). Each layer of the solenoid is taken as a thin plate. The diamagnetic shielding currents will be nearly parallel to the wire axes, so should be unperturbed in first order by subdivision of the "plate" into wires. The effective thickness of the plate $2w$ is taken as $(1\text{-}\Delta y)\pi/4$ times the wire diameter to equalize effective sectional areas. The factor $(1\text{-}\Delta y)$ corrects for spacing along the coil axis and is $(1\text{-}\Delta y)\sim 0.93$ for the present case.

A complete magnetization cycle may be obtained by starting with a specimen in a state $H_a=0$, $4\pi\bar{M}=0$, and applying the results of Eq. (3.3). It is assumed that: (1) $H=H_a$ at the specimen surface, (2) $B(x)=0$ initially throughout the specimen, and (3) changes occur only according to Eq. (3.3). Consequently the state of magnetization at interior points depends on magnetic history and is altered by applied field changes if and only if they are large enough to overcome the shielding of the interior points by the superconducting material nearer the specimen surface. Once an interior point has a current density characteristic of the critical state, it remains in the critical state as long as it is superconducting.

Figure 2 shows an average magnetization curve calculated using the relation $J_c=\alpha/(B+B_0)$. Corresponding curves can be computed for other critical-state equations, but all are qualitatively similar and this particular form is simple enough to be easily followed and complex enough to fit most of the experimental results. In Fig. 2, it can be seen that the average magnetization increases near (A) with applied field from the virgin state at the origin of the plot, completely enters the critical state between (A) and (B), and thereafter traces a critical-state curve (B)-(C)-(D)-(E)-(F), etc. Reversal of the direction of change of applied field as at (C) does not remove the specimen from the critical state but merely reverses locally the direction of the critical current, leading to a lower average magnetization. The sequence of Figs. 2(A)–2(E) show profiles of $B(x)$ at the corresponding points in Fig. 2 above.

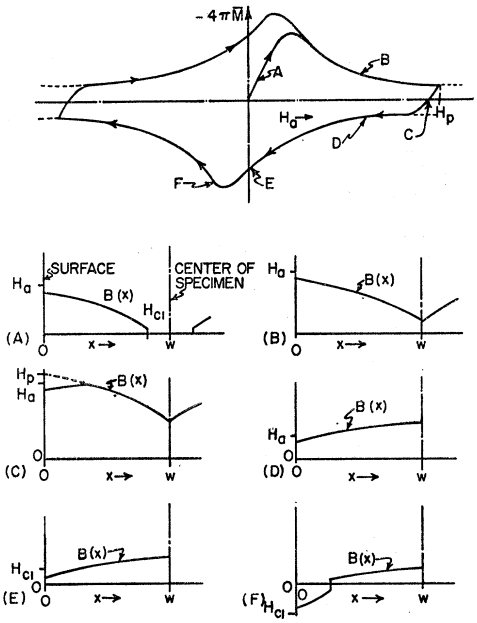

FIG. 2. A magnetization curve $4\pi M(H_a)$ calculated for a flat plate of thickness $2w$ with a critical-state equation of the form $J(B)=\alpha/(B_0+B)$ is shown at the top of the figure. Contours A-F show the magnetic induction $B(x)=H+4\pi\bar{M}(x)$ calculated for selected points along the magnetization curves indicated. The magnetization $4\pi\bar{M}$ is the value of $B(x)-H_a$ averaged over the specimen.

Analytical expressions are given in Table I as Eqs. (a) through (g) for the local values of magnetic induction $B(x)$ and the corresponding average magnetization, $4\pi\bar{M}$ for each region of the magnetization curve. These expressions assume the critical-state equation $J_c=\alpha/(B+B_0)$ and follow from the solutions of Eq. (3.3). They are applicable to any specimen geometry that can be approximated by a flat plate. Similar expressions for a multiply connected hollow cylinder are given by Kim *et al.*[3]

The effects of equilibrium magnetization $M_e(H_a)$ are included in these expressions in the term H_0. For fields less than H_{c1} on the initial magnetization curve the effect of M_e is to just cancel H_a so that $H_0=0$. At higher fields the effect of M_e is to shield slightly the bulk of the material by surface currents as shown in Fig. 2.

3.4. Determination of the Critical-State Equation

A useful general result can be found by consideration of regions of the magnetization curve where the internal-field distribution has no discontinuities except at the surface and possibly at the center of the specimen, such as in Figs. 2(B) and 2(D), and can be regarded as a slowly varying function of position. This specifically excludes the region of initial penetration where the gradients may be very sharp. With this restriction

TABLE I. Analytic expressions for the average magnetization of a flat plate of superconducting material with the critical-state equation $J_c[B]=\alpha/(B+B_0)$.

Region of validity	Average magnetization $4\pi\bar{M}=\frac{1}{\omega}\int_0^\omega [B(x)-H_a]dx$	
Increasing H_a $0\leq H_a\leq H_{c1}$	$4\pi\bar{M}=-H_a$	(a)
Increasing H_a $H_{c1}<H_a<[(B_0+H_{c1})^2+2\alpha k\omega]^{1/2}-B_0$ [Fig. 2(A)]	$4\pi\bar{M}=-H_a-\frac{(B_0+H_a)^2}{\alpha k\omega}\left\{\frac{B_0}{6}-\frac{H_a}{3}\right\}+\frac{(B_0+H_{c1})^2}{\alpha k\omega}\left\{\frac{B_0}{6}-\frac{H_{c1}}{3}\right\}$	(b)
Increasing H_a $[(B_0+H_{c1})^2+2\alpha k\omega]^{1/2}-B_0\leq H_a\leq H_p$ [Fig. 2(B)]	$4\pi\bar{M}=-(B_0+H_a)-\frac{1}{3\alpha k\omega}\{[(H_0+B_0)^2-2\alpha k\omega]^{3/2}-(H_0+B_0)^3\}$	(c)
Decreasing H_a $[(H_p+B_0)^2-4\alpha k\omega]^{1/2}-B_0\leq H_a\leq H_p$ [Fig. 2(C)]	$4\pi\bar{M}=-(B_0+H_a)+\frac{1}{3\alpha k\omega}\{2[H_0^2+2H_0B_0+H_p^2+2H_pB_0+B_0^2]^{3/2}-(H_0+B_0)^3-[(H_p+B_0)^2-2\alpha k\omega]^{3/2}\}$	(d)
Decreasing H_a $H_{c1}\leq H_a\leq[(H_p+B_0)^2-4\alpha k\omega]^{1/2}-B_0$ [Fig. 2(D)]	$4\pi\bar{M}=-(B_0+H_a)+\frac{1}{3\alpha k\omega}\{[(H_0+B_0)^2+2\alpha k\omega]^{3/2}-(H_0+B_0)^3\}$	(e)
Decreasing H_a $-H_{c1}\leq H_a\leq+H_{c1}$ [Fig. 2(E)]	$4\pi\bar{M}=-(B_0+H_a)+\frac{1}{3\alpha k\omega}\{[(B_0+H_{c1})^2+2\alpha k\omega]^{3/2}-(H_{c1}+B_0)^3\}$	(f)
Decreasing H_a $B_0-[(B_0-H_{c1})^2+2\alpha k\omega]^{1/2}\leq H_a\leq-H_{c1}$ [Fig. 2(F)]	$4\pi\bar{M}=\frac{1}{3\alpha k\omega}\{[2(B_0+H_{c1})^2-(B_0+H_0)^2+2\alpha k\omega]^{3/2}-(B_0-H_0)^3\}+\frac{B_0}{\alpha k\omega}\{(B_0-H_0)^2-(B_0+H_{c1})^2\}$	(g)

$J_c(x)$, which is an even more slowly varying function of position, can be expanded in a MacLaurin series about $x=0$, and the magnetization can be found with the help of Eqs. (3.1) and (3.3).

If plus and minus superscripts denote the two branches of the magnetization curve, with minus indicating the increasing applied field branch which has a negative magnetic moment, the following series expressions are obtained after two integrations:

$$4\pi(\bar{M}^+-\bar{M}^-)=kwJ(H_a)+\frac{kw^2}{3!}\left[\left(\frac{\partial J}{\partial x}\right)_0^+-\left(\frac{\partial J}{\partial x}\right)_0^-\right]+\cdots, \quad (3.4)$$

$$4\pi(\bar{M}^++\bar{M}^-)=2(4\pi M_e)+\frac{kw^2}{3!}\left[\left(\frac{\partial J}{\partial x}\right)_0^++\left(\frac{\partial J}{\partial x}\right)_0^-\right]+\cdots, \quad (3.5)$$

where the notation on the partial derivatives indicates the branch of the magnetization curve with which the current is associated and that it is to be evaluated at $x=0$.

If all terms but the first in Eqs. (3.4) and (3.5) are neglected, the experimentally determined values of $\bar{M}^+$ and $\bar{M}^-$ yield first approximations for $4\pi M_e$ and $J_c(H_a)$. An iterative process can then be used to obtain these expressions to accuracy limited only by the experimental data.

As an illustration, using the critical-state equation $J_c=\alpha/(B+B_0)$, as in Sec. 3.3, Eqs. (3.4) and (3.5) become

$$4\pi(\bar{M}^++\bar{M}^-)=2(4\pi M_e)-(\alpha kw)^2/3(B_0+H_0)^3+\cdots, \quad (3.6)$$

$$4\pi(M^+-M^-)=\alpha kw/(B_0+H_0)+(\alpha kw)^3/4(B_0+H_0)^5-\cdots, \quad (3.7)$$

which may be verified by expanding Eqs. (c) and (e) of Table I in powers of $\alpha kw/(B_0+H_0)^2$ and combining.

3.5. Experimental Observations of the Critical State

Inherently nonuniform magnetization is a characteristic of the critical state. However, the preceding sections connect the local values of magnetic induction determined by a critical-state equation with an average magnetization $4\pi\bar{M}$ that is characteristic of the entire specimen and thus measurable as outlined in Sec. 2. It should be emphasized that the values of $\bar{M}(H_a)$ and correspondingly of $d\bar{M}/dH\equiv\bar{\chi}_\Delta(H_a)$ depend on specimen geometry and that the appropriate material parameters are the constants of the critical-state equation $J(B)$ and the equilibrium magnetization $M_e(H_a)$.

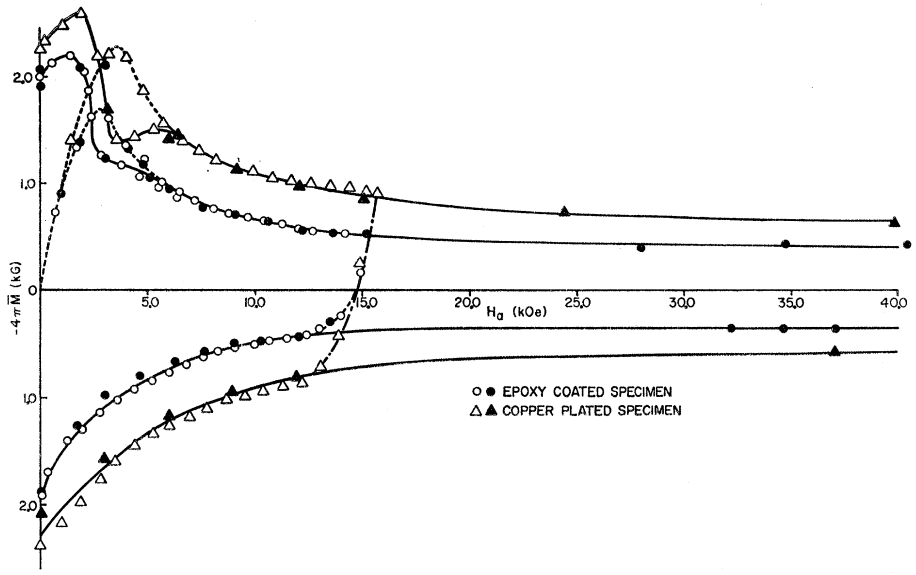

FIG. 3. Magnetization curves that give the "best fit" to the experimental data for both specimens are shown. The closed points represent data taken by thermal demagnetization during several runs. The open points show results from one typical run obtained by integration of differential susceptibility data. The critical-state hysteresis loops are indicated by solid lines; the initial magnetization regions where part of the specimen has not reached the critical state are indicated by dashed lines; and typical transition regions accompanying reversals of the direction of applied field change are indicated by chain curves. The results found for negative applied field indicate that the critical-state hysteresis loop is symmetrical under a 180° rotation about the origin of the plot. Successive cycles around the critical-state curve always reproduced the hysteresis loop.

4. RESULTS

4.1. Magnetization and the Critical State

4.1.1. Observations

All of the measurements of magnetization were generally consistent with the existence of reproducible hysteresis curves indicative of metastable critical states analogous to those discussed by Bean[1] and Kim, Hempstead, and Strnad[2] as developed in Sec. 3.1 of this paper.

Tests of two materials are reported: Namely (1) Nb–25%Zr wire of 0.010 in. diam produced and epoxy-insulated by the Westinghouse Electric Company and identified as lot SSC-32T, and (2) Nb–25%Zr wire produced by the Wa-Chang Corporation, and electroplated with about 0.001 in. of copper by the Summit Plating Company of Thomaston, Connecticut. Both samples represent typical commerical batches of wire that have displayed good performance in superconducting magnets.

Figure 3 shows "best-value" magnetization curves and several sets of typical data on the two materials.

The concurrence of data obtained by thermal demagnetization with that obtained by numerical integration of differential susceptibility measurements establishes the existence of a well-defined critical state. (Quantitative observations of the definitiveness of the critical state are discussed in Sec. 4.3.) The two samples of each material, one inductively wound, the other non-inductive, yielded indistinguishable magnetization results and are not reported separately.

All of the results confirmed the existence of an initial, reproducible magnetization curve for a "virgin" sample cooled below its transition temperature at $H_a=0$, that approached a reproducible critical-state hysteresis loop at $H_a\approx 5$ kOe. Repeated cycling to high fields reproduced closed hysteresis loops with twofold rotational symmetry about the origin. The chain portions of th curves display typical transitions between branches of the hysteresis curve on reversal of the direction of change of H_a. The small humps in the hysteresis loops at $H\approx 5$ kOe and $-4\pi\bar{M}\sim 1.5$ kG were fully reproducible; varying amongst runs only in detail. With this exception these results are consistent with the qualitative hysteresis loop below 10 kOe given by LeBlanc[12] for a different wire sample.

The Meissner effect was less than 100 G in these specimens as expected.

To test the geometrical assumptions the connectivity of the coils was changed by making a superconducting short circuit between the ends of the inductively wound spools of wire. This drastically changed their magnetic behavior. Now they excluded flux from the interior of the coils as do hollow superconducting cylinders. In this condition their magnetization curves could not be measured because their behavior was dominated by catastrophic transitions to the normal state at intervals of about 5 kOe.

More surprisingly, a specimen composed of a 5-mm-

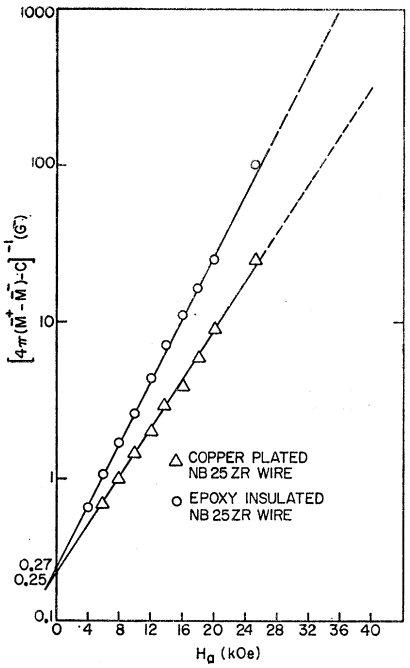

FIG. 4. Data used in determining the form of the critical-state equation. In the ordinate, $[4\pi(\bar{M}^+-\bar{M}^-)-c]^{-1}$, the quantity $4\pi(M^+-M^-)$ is the "width" of the magnetization loop at a given applied field and c is the apparent high-field limit of $4\pi(M^+-M^-)$. The resulting exponential form of the critical-state equation is given as Eq. (4.1) in the text.

diam bundle of straight, fully insulated Nb–25%Zr wires each about 5 cm long and aligned parallel to the applied field also underwent catastrophic transitions to the normal state. The reason for this behavior is not entirely clear but it does suggest the importance of geometrical factors.

4.1.2. Determination of the Critical-State Parameters

In Sec. 3.4 it was shown that the quantity $4\pi(\bar{M}^+-\bar{M}^-)/kw$ is approximately equal to $J_c(H_a)$, where $J_c(H_a)$ is the critical-state equation with $B(x)$ being replaced by $H_a+4\pi M_e$. Thus, approximate analytical forms for the critical-state equation can be found and inserted in Eq. (3.2) to obtain $B(x)$ and eventually $4\pi\bar{M}(H_a)$ in functional form. The fit of curves to the experimental data will test whether that derived critical-state equation is applicable. This is the program followed here in analyzing the data.

Initially, a curve of the form $J(B)=\alpha/(B+B_0)$ was fitted to the medium field data (3–15 kOe). From the slopes and intercepts of a plot of $(4\pi\bar{M}^+-4\pi\bar{M}^-)^{-1}$ as a function of the applied field, the material parameters were found to be: For the copper plated coil, $\alpha=1.9\times10^6$ kG-A/cm^2 and $B_0=2.6$ kG; for the epoxy insulated coil, $\alpha=0.95\times10^6$ kG-A/cm^2 and $B_0=1.3$ kG.

However, this form of critical-state equation was inadequate in two respects. At high fields it required that the magnetization decrease to zero, whereas it was observed to level off at a constant value above ~15 kOe. Even for the small range of applied fields used to determine α and B_0, there is a definite systematic departure from the assumed form. Adding a constant to obtain a relationship of the form $\alpha/(B+B_0)+c$ still did not yield a reasonable fit to the experimental results.

Test of a few trial functions showed a remarkably good fit with

$$J_c=(a_0/b_0)\exp(-B/b_0)+c_0, \qquad (4.1)$$

which is a special case of the assumed general form of Eq. (3.1). Figure 4 is a semilogarithmic plot of the quantity $[4\pi(\bar{M}^+-\bar{M}^-)-kwc_0]^{-1}$ for both specimens. The quantity kwc_0 was determined by trial to give the best straight line fit, and is essentially the value of $4\pi(\bar{M}^+-\bar{M}^-)$ at high fields. The other two constants, a_0 and b_0 were determined from the intercepts and the slopes of the lines. The values obtained were: *copper plated coil*, $c_0=0.79\times10^5$ A/cm^2, $a_0/b_0=2.4\times10^5$ A/cm^2, and $b_0=3.6$ kG; *epoxy-insulated coil*, $c_0=0.48\times10^5$ A/cm^2, $a_0/b_0=2.3\times10^5$ A/cm^2, and $b_0=4.6$ kG.

The exponential form, Eq. (4.1), can be integrated in Eq. (3.3) to give the local magnetic induction $B(x)$ in closed form.

The second integration for the average magnetization $4\pi\bar{M}(H_a)$ yields an infinite series which converges rapidly in the range where the magnetization penetrates smoothly to the center of the specimen.

4.1.3. Critical Transport Currents

The critical transport currents of the bifilar specimen coils were determined as a function of applied field. For each measurement the applied field was raised to a fixed value, then the transport current was increased until a resistive transition occurred. If the corresponding critical average transport current densities $J_t(H_a)$ are determined by critical-state criteria, $J_t(H_a)$ should

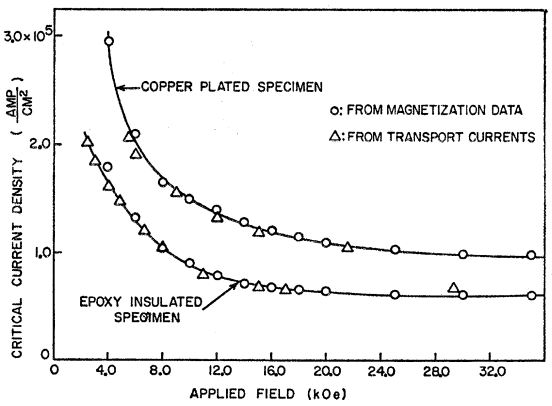

FIG. 5. Critical-current densities in two specimens comparing $J_t(H_a)$ from critical-transport current data and $J_c(B)$ from magnetization data.

equal the critical-current densities $J_c(B)$ determined from the magnetization measurements to a good approximation above $H_a=4$ kOe. Figure 5 shows the good agreement of critical-state magnetization currents in both specimens and demonstrates the dependence of critical transport currents on the critical-state parameters. The transport currents reported are the values attained after training in those ranges where training occurred. (Training and magnetization changes during training in these specimens will be described in a later paper.)

4.2. Equilibrium Magnetization

The equilibrium magnetization above 4 kOe can be deduced from the anisotropy of the magnetization data with the help of Eq. (3.6). For comparison, the theoretical equilibrium magnetization curve can be computed from the theory of Abrikosov,[6] using BCS theory[17] and relations due to Gor'kov[18] in deducing the parameters. The observations of specific heat γ and critical temperature T_c, reported by Morin and Maita[19] yield values appropriate to Nb-25%Zr of $\gamma=36\times10^4$ cal-deg^{-2}-mole^{-1} and $T_c=10.9$°K. Using a measured normal resistivity, $\rho=31.5\times10^{-6}$ Ω-cm yields $\kappa=26.1$, $H_c=2240$ Oe, $H_{c1}=210$ Oe, and $H_{c2}=83\,000$ Oe at 4.2°K. By numerical integration near H_{c1} and extrapolation from H_{c2} an approximate reversible magnetization curve was obtained and is shown in Fig. 6 along with the experimental values of equilibrium magnetization calculated from Eq. (3.6). The value of M_e calculated from Abrikosov's[6] theory just accounts for all the high-field asymmetry of the magnetization curve.

4.3. Definitiveness of the Critical State

The dependence of $\bar{\chi}_\Delta$ on the sign and magnitude of the applied field increments ΔH, provides an effective measure of the "sharpness" of the critical state. Figure 7 shows the dependence of the apparent differential susceptibility $\bar{\chi}_\Delta=\Delta\bar{M}/\Delta H$ on the magnitude of ΔH_a at a particular point along the hysteresis curve. The value observed at this field point during continuous field variation is also indicated. It appears that there is an uncertainty of about 30 G cm^2 in the magnetic moment change due to these increments. For applied field increments of 30 G several successive applied field increments are required before the expected behavior appears. This effect is most pronounced at low fields along the hysteresis loop as can be seen in the differential susceptibility. In Fig. 7 some values of χ_Δ for $\Delta H\cong30$ G are compared with the highly reproducible results obtained with $\Delta H_a\cong600$ G. Complete sets of χ_Δ data with $\Delta H_a\cong600$ G appear in Fig. 8. The region of highest instability is recognizable in Fig. 9 where a direct tracing of $\bar{M}(H_a)$ is presented as the output of an integrator circuit. Substantial flux jumps are apparent at low fields. The unstable region is just the region where local magnetization profiles like that of Fig. 2(F) are expected. Here there is an internal interface between adjacent regions of opposite magnetization. This suggests that magnetization changes occur here by mutual annihilation of fluxoids of opposite orientation. Erratic flux jumping might be expected to be a characteristic of this reaction.[20] This region of the data of Fig. 3 appears smooth in this less sensitive record; the flux jumps visible in Fig. 9 are ~600 G cm^2.

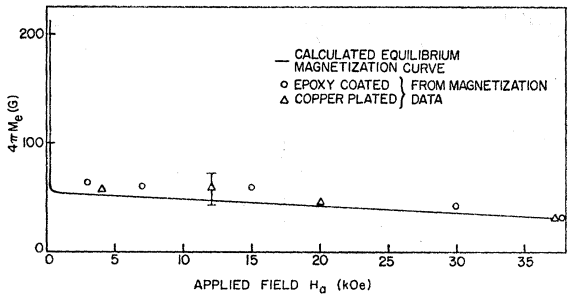

FIG. 6. The equilibrium magnetization curve as calculated from the theory of type-II superconductors. The points shown are calculated from the asymmetry of the experimental magnetization curve according to Eq. (3.6).

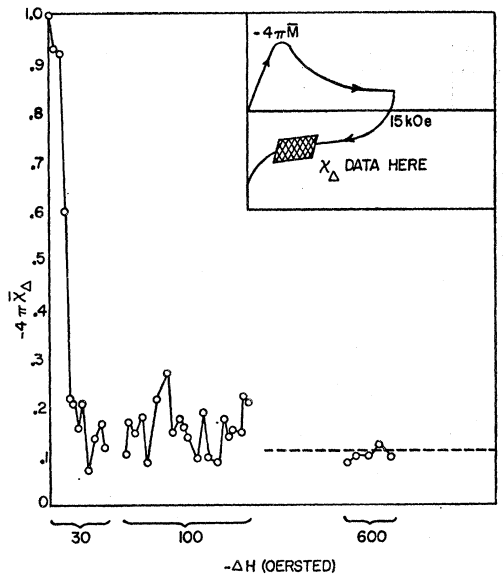

FIG. 7. The dependence of the differential susceptibility on the size of the applied field increment. Points are in sequential order from left to right and represent a continuation of the curve shown in the inset after pausing at that point long enough to ensure thermal equilibrium. The horizontal dashed line is the differential susceptibility at this point as seen by the electronic integrator with the applied field continuously changing at a rate of 100 Oe/sec.

[17] J. Bardeen, L. N. Cooper, and J. R. Schreiffer, Phys. Rev. 108, 1175 (1957).
[18] L. P. Gor'kov, Zh. Eksperim. i Teor. Fiz. 37, 1407 (1959) [English transl.: Soviet Phys.—JETP 10, 998 (1960)].
[19] F. J. Morin and J. P. Maita, Phys. Rev. 129, 1115 (1963).
[20] J. Silcox and R. W. Rollins, Rev. Mod. Phys. 36, 52 (1964).

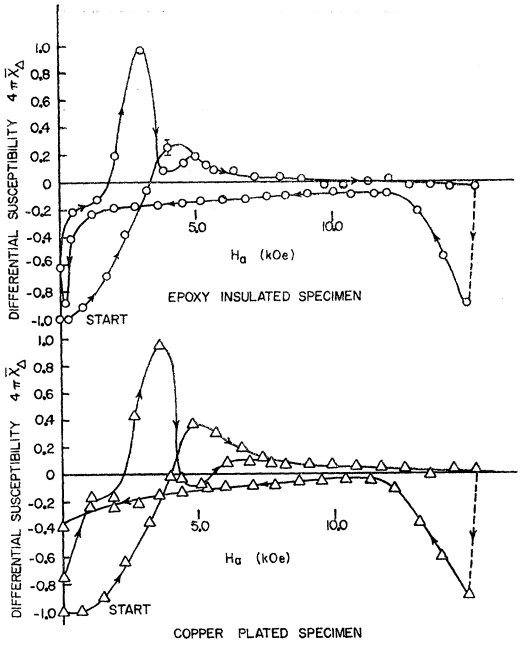

FIG. 8. Differential susceptibility $\chi_\Delta = d\bar{M}/dH$. The points on this curve were taken by incremental changes in the applied field and correspond to the points on Fig. 3. The error bar indicates instrumental and reading error of individual points.

Within the critical-state loop initial departures from the hysteresis curve on reversing the sign of ΔH always yielded apparent values of $\chi_\Delta \sim -1/4\pi$, that is, the magnetization changed diamagnetically in proportion to H, seemingly without hysteresis. On reapproaching a boundary of the loop, $4\pi\bar{M}$ gradually changed to become asymptotic to the loop as illustrated by the chain lines in Fig. 3. The behavior within the loop is more complex very near $H=0$ and is not considered here.

The behavior of the experimental magnetization curve up to 6 kOe increasing field on the hysteresis loop shows an extra dip and hump. This is just the region where erratic flux jumping occurs, and it may be that these flux jumps reduce the magnitude of the average magnetization below the regular critical-state curve. This observation is supported by the fact that the dip in the curve appears to be rate sensitive and was suppressed by rapidly changing the field through the unstable region. However, the possibility of a geometric effect cannot be entirely eliminated. The specimen geometry should be most disturbed here in the region of extreme values of dM/dH_a. Thus, the dip may be simply a manifestation of a change in the field at the specimen surface corresponding to a given applied field; that is, it may be a demagnetization effect.

5. SUMMARY AND DISCUSSION

5.1. Applicability of the Critical State

The magnetization and critical transport currents of samples of commercial Nb–25%Zr superconducting magnet wire have been measured and analyzed on the basis of the critical-state theory for hard superconductors. It proved necessary to modify the theory to include the reversible magnetization and the results clearly distinguish between the reversible magnetization and the hysteretic magnetization associated with high current-carrying properties. In addition good quantitative agreement has been found between average critical transport current densities $J_c(H_a)$ and the magnetization current densities $J_c(B)$ in the range of applied field 4–40 kOe. The observation of flux jumps and a measurable indefiniteness of the differential susceptibility also confirm the applicability of critical-state concepts to this material.

5.2. Equilibrium Magnetization

The equilibrium magnetization M_e does appear to contribute measurably to the total magnetization of Nb-25%Zr wire at high fields and in fact by just the amount predicted by Abrikosov's theory. The contribution between 4 and 40 kOe is about 50 G. In deducing the equilibrium magnetization, it was assumed to be independent of the critical-state magnetization and dependent only on the applied field. This assumption was not severely tested in the results because of the slow variations of M_e in the range where it is measurable.

5.3. Critical Transport Currents

Values of critical current densities determined from magnetization $J_c(B)$ and from critical transport currents $J_t(H_a)$ agree quantitatively above 4 kOe with no adjustable parameters in the comparison. Assumptions about the distribution of transport currents that are innocuous at high fields, make the comparison ambiguous at lower fields.

5.4. Critical-State Equations

The results indicate that the customary forms for the critical-state equation $J(B)$ do not fit the measured

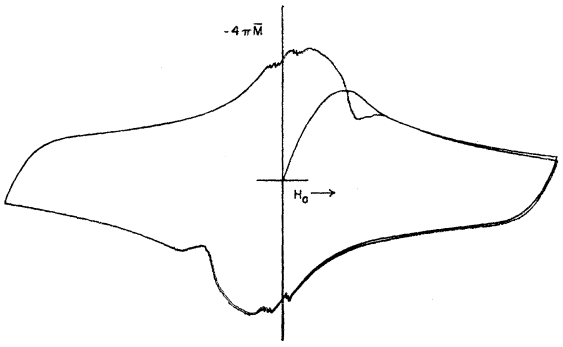

FIG. 9. Magnetization of the epoxy-insulated specimen as recorded by the electronic integrating circuit. The axes in this curve are not quite orthogonal.

results. The form $J(B)=(a_0/b_0)\exp(-B/b_0)+c_0$ chosen to fit the data in the range 4 kOe H_a to 40 kOe has no recognized fundamental physical significance. However, a universal form for critical-state equations should not be expected since they involve several factors, i.e., an electromagnetic force law, spatial variation of order parameter, effective concentration of pinning points and the effective strength of pinning points. Additional perturbations may arise due to surface effects and special interactions between adjacent regions with opposite directions of magnetic induction. Many hard superconductors, such as niobium and vanadium,[21] also seem to deviate from the usual critical-state equations.

A simple critical-state equation may suffice to describe a narrow range of applied fields but parameters so deduced may be a deceptive basis for comparison of materials. The data reported fit $J_c=\alpha/(B_0+B)$ between 4 and 16 kOe, but $J_c\cong$constant between 16 and 40 kOe and may well be more complex at still higher fields. This complicates the identification of pinning mechanisms, etc., with a particular critical-state equation. Values of α and B_0 deduced from low-field data in the present case are ambiguous because of uncertainty about the low-field limit of the plateau dominating the high-field magnetization (and transport) current densities.

5.5. Definitiveness of the Critical State

The measurements bearing on the definitiveness of the critical state are probably not simple manifestations of flux creep,[4] nor limitations of measuring equipment. The critical-state magnetization appears to become insensitive to step changes of applied field <30 Oe. This is particularly evident where $\bar{\chi}_\Delta/4\pi\bar{M}$ is positive and large. Rather modest flux jumps ~ 600 G cm^2 occur up to 4 kOe but were not detrimental to determination of the critical-state curve. However, flux jumps of this size in a magnet or in a multiply connected specimen might well grow to a catastrophic transition to the normal state. This possibility was confirmed by observations of "training" of the critical transport currents in just the regions of flux jump observations that will be reported later.

5.6. Methods of Measurement

The methods of magnetization measurement employed for the seemingly awkward spools of wire are entirely consistent with each other and accurate to $\sim\pm 5\%$ at least at high fields. At lower fields where the diamagnetism is comparable with the applied field, local field nonuniformities probably would smear out sharp changes of magnetization with applied field. The interaction between layers of the coil probably produces perturbations beyond other experimental error. It is possible that the dip in the critical-state curve near 4 kOe is due to geometrical effects.

The three magnetization measurement methods employed are complementary. Continuous electronic integration of the differential susceptibility is by far the most convenient scheme. Continuous incremental observations of $\bar{\chi}_\Delta$ are tedious but reliable and revealing of the definitiveness of the critical state. Thermal demagnetizations yield precise values of the magnetization that are essential for accurate calibration at a few points since any integration of the $\bar{\chi}_\Delta$ accumulates errors in $\bar{M}$.

Analysis of the critical-state magnetization revealed simple approximate formulas for conveniently obtaining M_e and $J_c(B)$ easily by comparing the high-field magnetization data in increasing and decreasing fields. The conditions under which $J_c(H_a)=J_c(B)$ seem to be sufficiently unrestrictive that this approximation will probably prove to be generally useful.

5.7. Comments on Superconducting Magnet Behavior

The low-field instabilities and the large differences between initial- and critical-state magnetization at low fields strongly suggest that it is the low-field portions of superconducting magnets made of Nb–25%Zr wire that is responsible for many of the well-known (and poorly documented) observations of behavior. The form of the magnetization and casual comparisons with the effects of metallurgical variables on critical transport currents suggests that more than one pinning mechanism is involved in establishing the critical-state equation and that the mechanisms predominating in low fields, on the plateau, in the peak and in the very high-field resistive region may all differ. The data show large differences between the copper-plated and the epoxy-coated specimens. However, it was not determined whether this is an effect of plating or a difference due to the alloys themselves.

ACKNOWLEDGMENTS

The authors gratefully acknowledge interesting conversations with R. W. Rollins and Dr. M. A. R. LeBlanc, the assistance of J. B. Sayah in carrying out the experimental work, the support of the U. S. Atomic Energy Commission, and the facilities of the Advanced Research Projects Agency at Cornell.

[21] Y. B. Kim, C. F. Hempstead, and A. R. Strnad, Phys. Rev. **131**, 2486 (1963).